Relationship between Inter-Symbol-Transition Pattern and Optical Filtering Performance for Multi-Level PSK Modulator Implementations

Yan Bingyang Yang Yanfu Zhong Jiechang Zhu Yupeng Cao Jianchao Yao Yong

(*Department of Electronic and Information Engineering, Shenzhen Graduate School, Harbin Institute of Technology, Shenzhen, Guangdong* 518055, *China*)

Abstract The inter-symbol-transition (IST) patterns of multi-level non-return-to-zero phase-shift-keying (NRZ-PSK) signals generated by two kinds of optical modulator implementations are analyzed to reveal the underlying relationship between IST patterns and optical filtering performance. In the tandem modulator implementations, some IST patterns are curved, and in the parallel implementations, all IST patterns are inherently straight lines. It's proved that these IST patterns characteristics play a significant role in determining optical filtering performance. In the tandem implementations, optical filtering can lead to obvious IST pattern dependent signal distortion. As a comparison, the parallel implementations have less filtering-induced eye-opening penalty and consequently better tolerance against narrow filtering. Finally, the receiver sensitivity as a function of optical filter bandwidth for differential optical detection is studied together with the optimization of the demodulator parameter.

Key words optical communications; inter-symbol-transition pattern; spectral efficiency; phase-shift-keying; narrow filtering

OCIS codes 060.2330; 060.5060; 100.5090

多级相移键控调制器的码间跃变图案及滤波特性

颜丙阳 杨彦甫 钟杰昌 朱宇鹏 曹剑超 姚 勇

(哈尔滨工业大学深圳研究生院电子与信息工程学院，广东 深圳 518055)

摘要 分析了由两种光调制结构产生的高阶调相非归零码的码间跃变图案，并以此来研究码间跃变图案与光滤波性能间的关系。串行调制器方案下，部分跃变图案为曲线型，而在并行调制器方案下，所有的码间跃变图案本征均为直线型。可以证明，码间跃变图案特性对光滤波特性存在重要影响。在串行调制器方案下，光滤波可以导致明显的跃变图案依赖性。相对而言，并行调制方案有更小的眼睁开代价，因此具有更好的窄带滤波容忍性。最后，研究了在解调器参数优化下接收机灵敏度随光滤波带宽的变化曲线。

关键词 光通信；码间跃变图案；谱效率；相移键控；窄带滤波

中图分类号 TN913.7 **文献标识码** A **doi**：10.3788/CJL201441.s105008

1 Introduction

Various advanced modulation formats have been employed for achieving high spectral efficiency (SE) in dense wavelength-division-multiplexing (DWDM) systems. Differential quadrature phase-shift-keying (DQPSK)[1] combined with polarization division multiplexing (PDM) has already been utilized to obtain long-haul and large-capacity transmission systems[2]. Recently, with bandwidth demand drove by increasing internet traffic, many enabling technologies have been proposed to enhance SE further. In the transmitter, various novel modulator implementations have been proposed to generate multi-level phase-shift-keying (PSK) signals[3-6] or quadrature amplitude modulation (QAM) signals[7-8]. In the receiver, coherent optical detection and digital signal processing are employed for

收稿日期：2013-10-07；**收到修改稿日期**：2013-11-14

基金项目：国家自然科学基金(61205046)、深圳市战略性新兴产业发展专项资金(JCYJ20120613150130014)、哈尔滨工业大学科研创新基金(HIT.NSFIR.2011131)

作者简介：颜丙阳(1988—)，男，硕士研究生，主要从事先进光调制格式及相干光接收方面的研究。E-mail：ybyhitszfly@gmail.com

导师简介：杨彦甫(1981—)，男，博士，副教授，主要从事高速光通信系统及网络方面的研究。E-mail：yangyanfu@hotmail.com (通信联系人)

recovering amplitude and phase information simultaneously from channel-impaired signals. The tolerance against tight optical filtering[9] is one of the important issues for considering transmission impairments due to inter-symbol interference (ISI) resulted from cascading reconfigurable optical add-drop multiplexers[8]. Optical equalization[10] can be utilized to relax filtering tolerance with the penalty of the cost increment and additional insertion loss. Although digital equalization in electrical domain is flexible to restore signal from spectral narrowing, the existing algorithms have their own limitations in practice. Adaptive finite impulse filters based on equalization has the disadvantage of noise enhancement, and the sequence estimation methods with memory length require complex calculations in spite of their strong capability of suppressing ISI[11-12]. Therefore, it's fundamental to enhance the inherent optical filtering tolerance of optical signals by the optimization of the modulator implementations. This paper will investigate the dependence of optical filtering characteristics on modulator implementations for multi-level PSK optical signals and subsequently provide meaningful considerations on ideal modulator implementations to generate filtering-tolerated signal based on the framework of current available materials and processing technologies.

In this paper, the concept of inter-symbol-transition (IST) pattern is introduced to analyze the underlying influence of optical PSK modulator implementations on their generated signals' filtering characteristics. Firstly, two kinds of modulator implementations for multi-level NRZ-PSK signals are presented together with the simulation model. Then the generated IST patterns for these implementations are compared with theoretical analysis and numerical simulation. Finally, the influence of the IST patterns on optical filtering characteristics for two kinds of modulator implementations is investigated thoroughly. The main novelty of this paper is providing a unique view to investigate the modulator implementation dependence of tight filtering tolerance with the concept of IST pattern, and presenting the meaningful discussions on the optimal IST pattern to achieve the filtering-tolerated complex modulated signals for the use in future ultra-high SE optical networks.

2 Multi-level PSK modulator implementations

Figures 1(a) and (b) show the tandem QPSK modulator implementation and the parallel QPSK modulator implementation, respectively. The tandem QPSK implementation [Fig. 1(a)] consists of a push-pull Mach-Zehnder modulator (MZM) and a phase modulator (PM). The PM has the proper driving signal amplitude for $\pi/2$ phase deviation. The parallel QPSK implementation [Fig. 1(b)] is constructed by placing two parallel MZM on two arms of a Mach-Zehnder (MZ) interferometer with the phase bias of $\pi/2$.

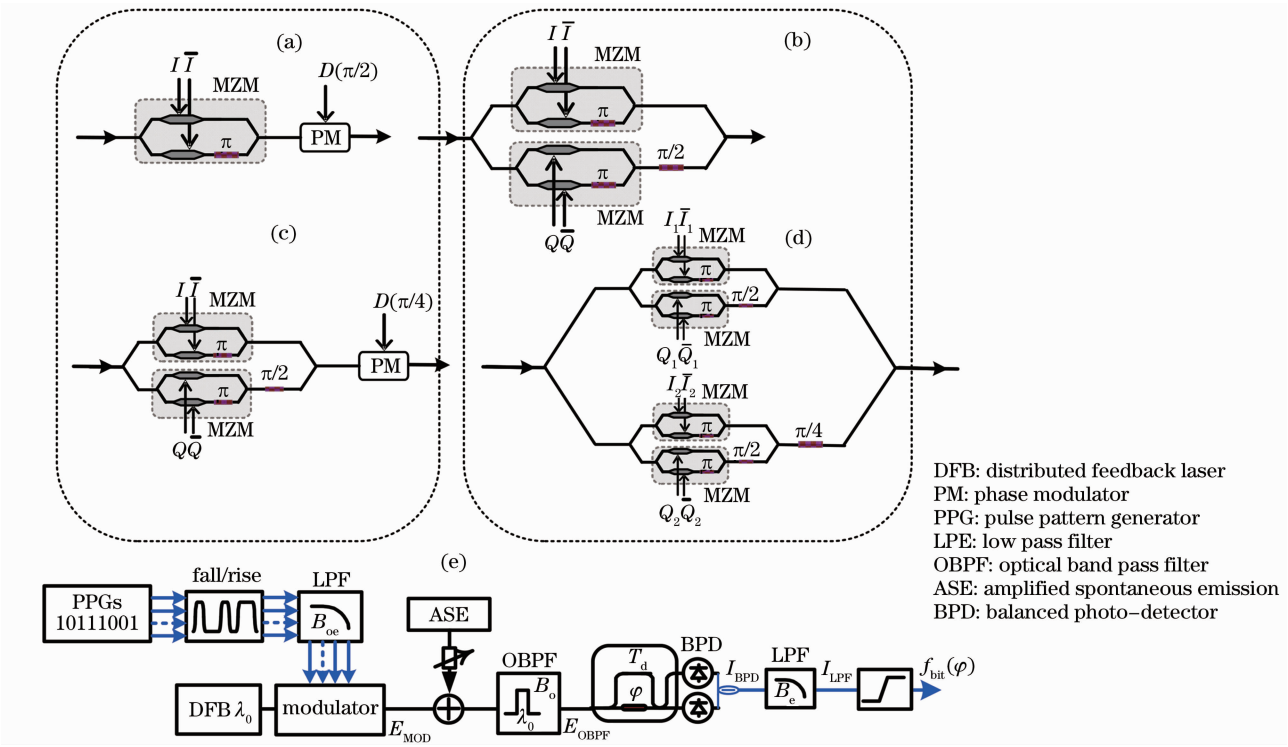

Fig. 1 Schematic implementations of (a), (b) QPSK optical modulators and (c), (d) 8PSK optical modulators; (e) simulation model

Figures 1(c) and (d) show the tandem and parallel 8PSK modulator implementation, respectively. The tandem-style 8PSK implementation [Fig. 1(c)] is obtained by concatenating a parallel QPSK modulator and a PM with the phase deviation of $\pi/4$. Fig. 1(d) shows the parallel 8PSK modulator implementation[3], in which two parallel QPSK modulators are placed in a MZ interferometer with the bias phase of $\pi/4$.

Figure 1(e) presents the system model for simulation. Multiple bit sequences from pulse pattern generators (PPGs) are custom-defined so that the generated optical symbol sequence has the feature of pseudo-random. This consideration is critical to take the filtering-induced ISI into account reasonably. The electrical signals from the PPGs have the fixed rise/fall time of one quarter of the symbol period (SP) of T. A 3rd-order Bessel electrical low-pass filter (LPF) with the fixed cutoff frequency B_{oe} of $0.9/T$ is used to simulate the limited bandwidth of the driver amplifiers and the modulators. The amplified spontaneous noise (ASE) with variable power is coupled with the modulated signal to adjust optical signal-to-noise ratio (OSNR). The following optical band-pass filter (OBPF) has 3rd Gaussian transmission profile, which has adjustable 3 dB bandwidth B_o. At the receiving end, direct differential detection is used with the delay-line demodulator, which has the time delay T_d and the phase offset φ. The electrical Bessel LPF after the balanced photo-detector (BPD) has the fixed bandwidth of $0.75/T$. $f_{bit}(\varphi)$ represents the recovered bit stream after decision, in which φ can be one of $\{\pi/4, -\pi/4\}$ or $\{3\pi/8, \pi/8, -\pi/8, -3\pi/8\}$ for QPSK and 8PSK respectively[13]. E_{MOD} and E_{OBPF} represent optical electrical fields after the optical modulator and the OBPF, respectively. I_{BPD} and I_{LPF} represent the electrical signal after the BPD and the subsequent LPF, respectively.

3 Analysis on IST pattern and filtering characteristics

In this section, the IST patterns of the generated PSK signals by two kinds of modulator implementations are analyzed. The complex amplitudes of the generated optical signals are presented in Fig. 2. Note that S_i represents the symbols of optical QPSK/8PSK signals.

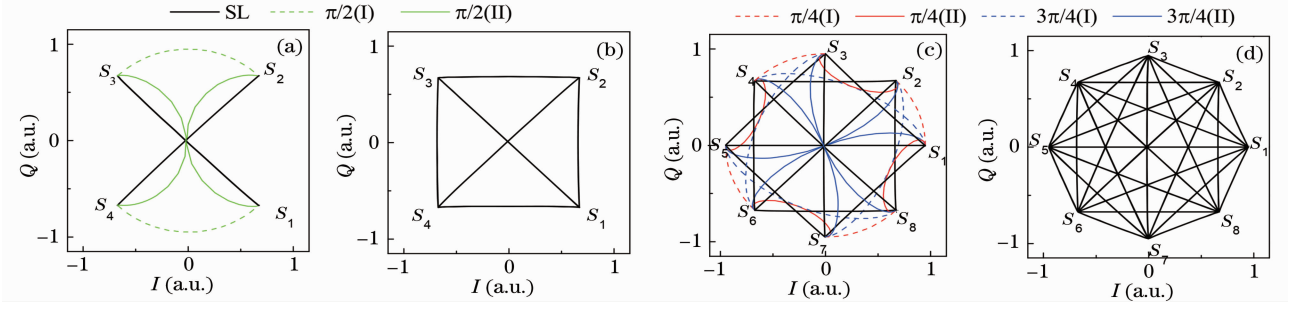

Fig. 2 Complex optical fields of the PSK signals generated by four modulator implementations, shown in Figs. 1(a)~(d) respectively

In the parallel-style modulator implementations, the resultant IST patterns [Figs. 2(b) and (d)] are straight lines (SL) for all possible differential phases. Through the following analytical derivation, the SL pattern can be directly contributed to the parallel-style modulator structure, in which multiple push-full MZMs are superimposed in parallel manner with the respective phase shifts. The output optical electrical field $E_{MOD}(t)$ can be represented as:

$$E_{MOD}(t) = A_0 \cdot \sum_{j=1}^{N} E_j(t) \cdot \exp(i\theta_j), \quad t \in [0, T], \tag{1}$$

where A_0 is a coefficient proportional to the average optical power after the modulator, N is the number of the involved push-pull MZMs and can be 2 or 4 for QPSK and 8PSK modulator implementations, $E_j(t)$ represents the output optical electrical field for the jth MZM, θ_j represents the phase shift imposed on $E_j(t)$ before superimposition, and T represents the symbol period.

Considering that the jth MZM is driven by binary electrical signal, there should be four possible bit transitions: $\{1 \to 1;\ 0 \to 0;\ 0 \to 1;\ 1 \to 0\}$ and consequently four profiles for $E_j(t)$ from one symbol center to the next. Because of the push-pull operation for the MZM, the resultant $E_j(t)$ is intrinsically chirp-free and can be represented by real-value functions. We assume that $E_j(t)$ has the constant value of 1 and -1 if the transition is $1\to1$ and $0\to0$, respectively, and has two real-value function of $P_{10}(t)$ and $P_{01}(t)$ for the transition of $0\to1$ and $1\to0$, respectively. Assuming that the driver binary signals have the symmetrical rising and falling traces, $P_{01}(t)$ has the relation to $P_{10}(t)$ as follows:

$$P_{10}(t) = P_{01}(T-t) = -P_{01}(t), \quad t \in [0, T]. \tag{2}$$

With the equations (1) and (2), the ratio between the first derivative of the real and imaginary part of the $E_{\mathrm{MOD}}(t)$ with respect to the time t is derived as follows

$$\frac{\mathrm{d}\{\mathrm{Re}[E_{\mathrm{OUT}}(t)]\}/\mathrm{d}t}{\mathrm{d}\{\mathrm{Im}[E_{\mathrm{OUT}}(t)]\}/\mathrm{d}t}=\frac{\mathrm{Re}\left[\sum_{j=1}^{N}\mu_j\cdot\exp(\mathrm{i}\theta_j)\right]}{\mathrm{Im}\left[\sum_{j=1}^{N}\mu_j\cdot\exp(\mathrm{i}\theta_j)\right]}=c,$$

$$t\in[0,\ T], \tag{3}$$

where c is constant value, μ_j can be $\{0,\ 0,\ 1,\ -1\}$ when $E_j(t)$ has the expression of $\{1,\ -1,\ P_{01}(t),\ -P_{01}(t)\}$, respectively. Obviously, the result only depends on the constant value of μ_j and θ_j and is regardless of t. Therefore, it's theoretically proved that the IST traces of $E_{\mathrm{OUT}}(t)$ in complex plane are inherently straight lines.

However, under the tandem modulator implementations, some IST patterns are curved due to the introduction of phase modulator in the tandem manner. In Fig. 2(a), two curved IST patterns exist for $\pi/2$ differential phase and noted as $\pi/2$(I) and $\pi/2$(II), respectively. Similarly, there are also two curved patterns for $\pi/4$ and $3\pi/4$ differential phases, noted as $\pi/4$(I), $\pi/4$(II), $3\pi/4$(I) and $3\pi/4$(II), respectively. The phase curves of the curved IST patterns as a function of time are plotted together with that of the SL patterns for comparison. The horizontal axis of time is normalized to SP with the range from one symbol center to the next. The obvious undershoots or overshoots can be found for $\{\pi/4$(II), $\pi/2$(II), $3\pi/4$(II)$\}$.

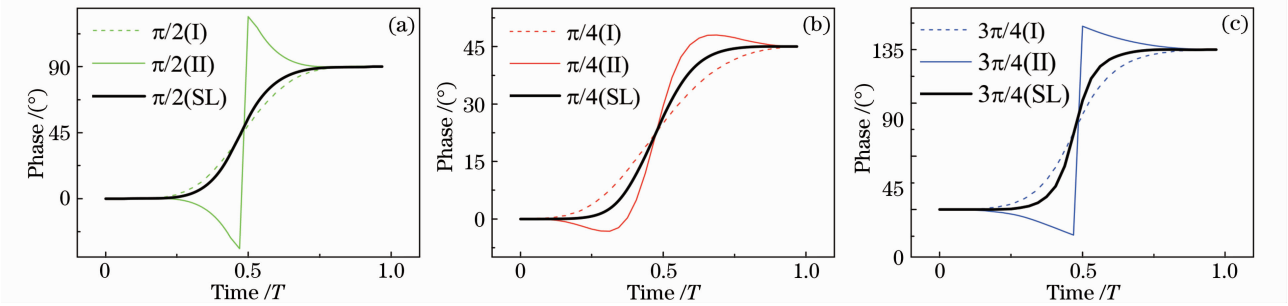

Fig. 3 Phase curves as a function of time for the differential phases of (a) $\pi/2$, (b) $\pi/4$ and (c) $3\pi/4$

For the same differential phase, different phase curves lead to different instantaneous frequency offsets as a function of time t. The differential phase between one symbol center and the next symbol center has the following relationship with the instantaneous frequency offset:

$$\psi_{n+1}-\psi_n=\int_0^T C(t)\mathrm{d}t=\underbrace{\int_0^{\Delta t}C(t)\mathrm{d}t}_{\text{start}}+\underbrace{\int_{\Delta t}^{T-\Delta t}C(t)\mathrm{d}t}_{\text{middle}}+\underbrace{\int_{T-\Delta t}^{T}C(t)\mathrm{d}t}_{\text{end}}, \tag{4}$$

where ψ_{n+1} and ψ_n represent the respective phase at 0 and T, located at the centers of two neighboring symbols; $C(t)$ represents the instantaneous frequency offset as a function of t. Here $[0, T]$ is roughly divided into three integral regions: $[0, \Delta t]$, $[\Delta t, T-\Delta t]$, and $[T-\Delta t, T]$. The start and end regions are close to symbol center, and the corresponding frequency offset has dominant contribution on optical filtering induced distortion. Considering that these two regions are mirror-symmetrical with respect to $T/2$, so the start region is only shown in Fig. 4 with the time range of $[0, 0.3]$. Obviously, two curved IST patterns has larger frequency chirp than the SL pattern during the time region $[0, 0.25]$. This can be understood qualitatively as follows: the curved patterns have longer traces than the SL patterns, so the 'travelling' velocity of the signals would be larger in order to complete the whole journey from one symbol to the next symbol within the constant symbol period. This indicates that the curved patterns are expected to have larger frequency chirp on average. Besides, the second type of curved IST patterns is found to have the opposite frequency offset

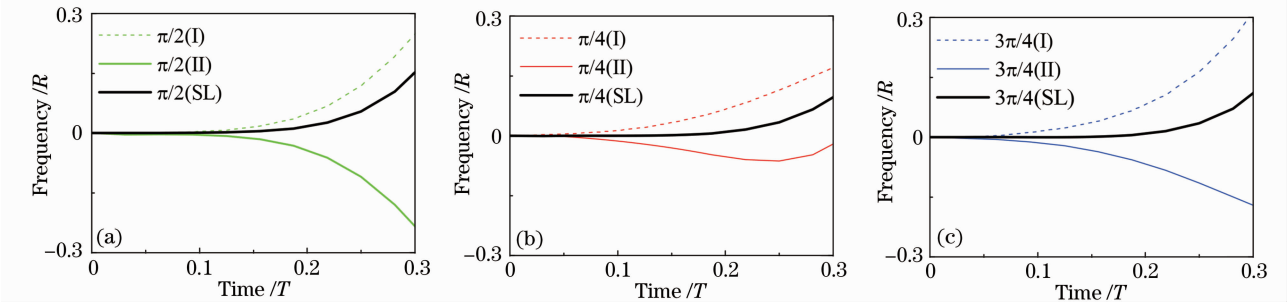

Fig. 4 Instantaneous frequency offsets under the differential phases of (a) $\pi/2$, (b) $\pi/4$ and (c) $3\pi/4$

to the first type of the curved patterns.

In the following, we will study how these IST patterns have a significant influence on optical filtering characteristics for two kinds of modulator implementations. Figure 5 presents the constellation diagrams of $E_{\mathrm{OBPF}}(nT)$ when the OBPF has 3 dB bandwidth of 1.2 symbol rate (SR, R). The root mean squares (RMS) of error vector magnitudes (EVM) in Figs. 5(a)~(d) are calculated to be 9.81%, 3.50%, 6.89% and 3.61%, respectively. The parallel implementations have less filtering-induced distortion than the tandem implementations under both QPSK and 8PSK cases. This can be mainly attributed to the fact that the SL patterns in the parallel implementation introduce less frequency chirp around symbol center than the curved patterns in the tandem ones.

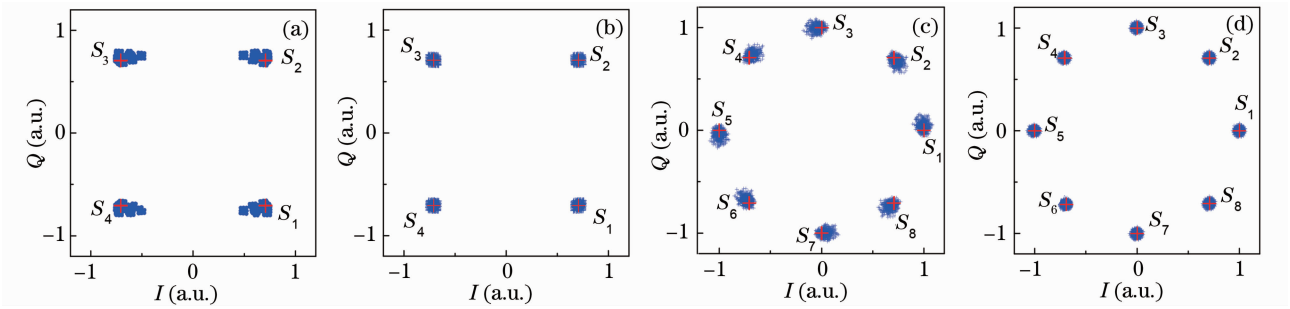

Fig. 5 Constellation diagrams of the signal $E_{\mathrm{OBPF}}(nT)$ when the modulator implementations in Figs. 1(a)~(d) are employed, respectively. $E_{\mathrm{OBPF}}(nT)$ is the filtered signal after the OBPF; signal $E_{\mathrm{OUT}}(nT)$ before the OBPF is also plotted as red crisscross as reference; n is an integer

Meanwhile, some interesting phenomenon can also be found in case of the tandem implementations [Figs. 5(a) and (c)]. The first one is that the distortion profiles of the signal symbols in complex plane are asymmetric with respect to ideal symbol location (marked by red crisscross). This is directly related to the topologies shown in Figs. 2(a) and (c), which are asymmetric with respect to the arrowed line from origin to S_i. The second one is that the cluster profiles around S_i can be classified into two groups based on its orientation. In Fig. 5(a), the clusters around S_1 and S_3 belong to a group and the clusters around S_2 and S_4 belong to the other. Similarly in Fig. 5(c), the clusters around $\{S_i,\ i=1,3,5,7\}$ and $\{S_i,\ i=2,4,6,8\}$ have their respective orientations. These results are also a direct consequence of the topology features shown in Figs. 2(a) and (c). With the criterion of surrounding IST patterns, $\{S_1, S_3\}$ belongs to one group and $\{S_2, S_4\}$ belongs to another. Similarly in Fig. 2(c), two classified groups are $\{S_i,\ i=1,3,5,7\}$ and $\{S_i,\ i=2,4,6,8\}$.

Differential detection is commonly used in high-order PSK optical communications for avoiding phase ambiguity. Therefore, it is important to analyze the distortion of the differential signal between two neighboring symbols. Figure 6 presents the constellation diagrams of $E_{\mathrm{OBPF}}(nT+T)*\mathrm{conj}[E_{\mathrm{OBPF}}(nT)]$ with four modulator implementations [Figs. 1(a)~(d)] employed, where conj[•] represents the conjugation operation. It's obvious that the distortion under the tandem implementations is more severe than that under the parallel ones. Besides, the clusters split into two parts for some specific differential phases in the tandem implementations. In Fig. 6(a), the clusters with the differential phase of $\pm i\pi/2$ split into two. It has been confirmed by simulations that two separate clusters generated when the IST patterns between symbols are $\pi/2$(I) and $\pi/2$(II), respectively. Similarly, two curved patterns for the differential phases of $\pi/4$ or $3\pi/4$ lead to separate clusters, as shown in Fig. 6(c).

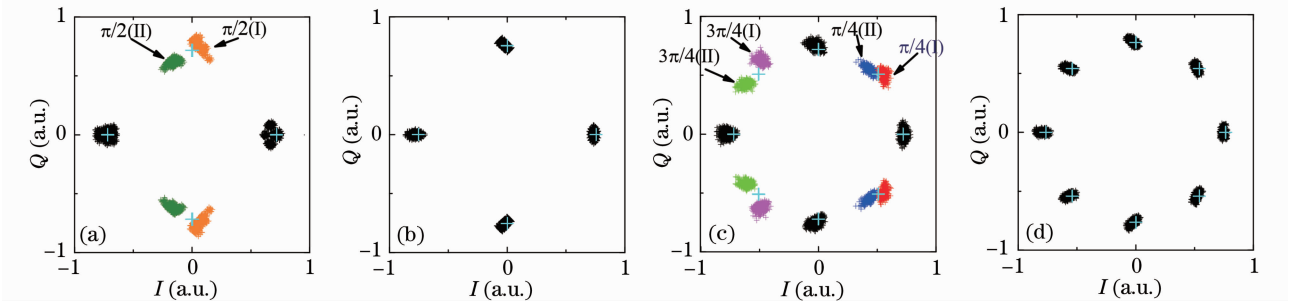

Fig. 6 Constellation diagrams of $E_{\mathrm{OBPF}}(nT+T)*\mathrm{conj}[E_{\mathrm{OBPF}}(nT)]$ with four modulator implementations shown in Figs. 1(a)~(d), respectively. $E_{\mathrm{OUT}}(nT+T)*\mathrm{conj}[E_{\mathrm{OUT}}(nT)]$ is also plotted as red crisscross as reference; n is an integer

Through the above analysis, it can be concluded that the modulator implementation inherently determines the characteristics of the IST patterns and their phase and frequency transition curves. In the parallel implementations, the IST patterns are all straight lines. However, in the tandem implementations there exist multiple curved IST patterns for one differential phase. This intrinsic IST pattern differences between two kinds of implementations theoretically determine optical filtering performance of their generated signals.

4 Simulation results and discussions

In the following section, optical filtering performances of QPSK and 8PSK generated by two kinds of modulator implementations are investigated by detailed simulations for practical differential direct receiver. Figures 7(a) and (b) show the contour plots of OSNR sensitivity [at bit error rate (BER) of 1×10^{-3}] as a function of the optical filter bandwidth and the delay time of the delay-line demodulator for the tandem and parallel QPSK modulator implementations, respectively. With the filter bandwidth of $1.0R$, the tandem implementation [Fig. 7(a)] has the penalty of 1.5 dB and 1.3 dB when the the delay time is set to one symbol period and the optimized $0.87R$, respectively. Consequently, 0.3 dB sensitivity improvement is achieved through the delay time optimization. The quantitative mechanism behind this improvement can be explained as a direct consequence of optical equalization resulting from increased free spectral range (FSR) transfer function[14]. In Fig. 7 (b), the parallel implementation has better tolerance against optical filtering compared to the tandem one. With the optimization of the delay time, the parallel implementation has nearly no penalty with the filter bandwidth of $1.0R$ and has only 0.5 dB penalty for $0.9R$ filter bandwidth. In term of the receiver OSNR sensitivity, the parallel and the tandem implementations have 14.5 dB and 15.6 dB after optimization, indicating that the former has 1.4 dB OSNR gain compared to the latter.

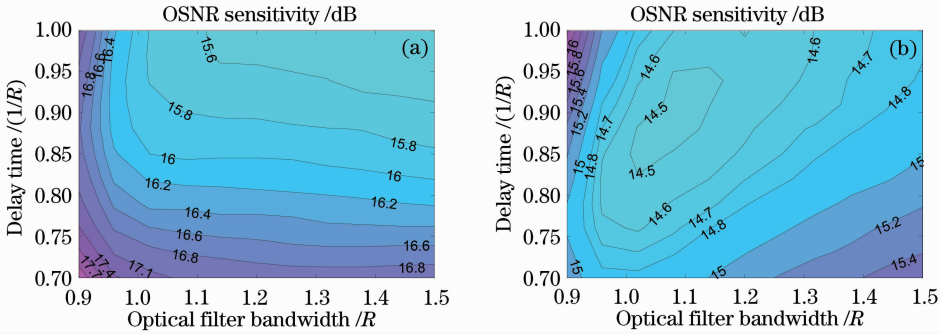

Fig. 7 Receiver OSNR sensitivity as a function of the delay time and the optical filter bandwidth for (a) the tandem QPSK modulator implementation and (b) the parallel QPSK modulator implementation

Figures 8(a) and (b) show the contour plots of OSNR sensitivity (at BER of 1×10^{-3}) as a function of the OBPF filter bandwidth and the delay time of the delay-line demodulator for the tandem and parallel 8PSK modulator implementations, respectively. With the tandem implementation, the optimal OSNR sensitivity is achieved with B_o of $1.45R$ and exacts one symbol delay. With B_o decreasing from $1.2R$ to $1.0R$, the OSNR sensitivity degrades rapidly. The sensitivity penalty is larger than 1.6 dB for B_o of $1.0R$ even with the optimized delay time around $0.87R$. As a comparison, the parallel implementation has excellent filtering performance and the delay time optimization has played a significant role in enhancing the filtering tolerance. With B_o decreasing from $1.3R$ to $1.1R$, the OSNR sensitivity is almost not degraded with the help of

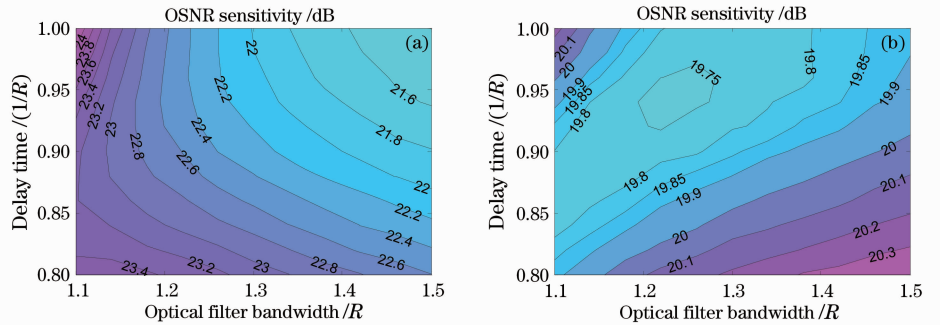

Fig. 8 Receiver OSNR sensitivity as a function of the delay time and the optical filter bandwidth for (a) the tandem 8PSK modulator implementation and (b) the parallel 8PSK modulator implementation

the optimized time delay. There even exists a slight sensitivity improvement by 0.3 dB when B_o decreases from $1.5R$ to $1.3R$ due to the enhanced suppression on out-of-band ASE. The parallel implementation has the better receiver OSNR sensitivity by around 1.85 dB compared with the tandem one. The former and the latter achieve their optimal sensitivity of around 21.6 dB and 19.75 dB respectively.

Therefore, the parallel implementations have better tolerance against narrow optical filtering than the tandem implementations. This can be intrinsically contributed to IST pattern characteristics between the signals generated by the tandem and parallel implementations, as analyzed in the prior section.

5 Conclusion

The relationship between the IST pattern and optical filtering performance under two kinds of multi-level optical PSK modulator implementations is analyzed theoretically and investigated by numerical simulation. The parallel implementations can generate PSK signals with the straight lines IST patterns, which introduces less frequency chirp around symbol centre. However, there are curved IST patterns in the case of the tandem implementations. Besides, there may be multiple patterns for one differential phase, which can induce the strong IST pattern dependent distortion under optical filtering. In term of the receiver sensitivity, the parallel implementations have advantage of 1.4 dB and 1.85 dB compared with the tandem ones for QPSK and 8PSK, respectively. Meanwhile, it's found that in the parallel implementations, the delay time optimization is more significant in enhancing OSNR sensitivity. This paper implements a comprehensive investigation on the connection between optical filtering performance and the modulator implementation dependent IST pattern and provides meaningful results for designing high-order optical modulator implementations for application in future high-SE optical transmission systems.

References

1 A H Gnauck, P J Winzer. Optical phase-shift-keyed transmission[J]. J Lightwave Technol, 2005, 23(11): 115-130.

2 G Charlet, J Renaudier, H Mardoyan, *et al*.. Transmission of 16.4-bit/s capacity over 2550 km using PDM QPSK modulation format and coherent receiver[J]. J Lightwave Technol, 2009, 27(3): 153-157.

3 T Sakamoto, A Chiba, T Kawanishi. Electro-optic synthesis of 8PSK by quad-parallel Mach-Zehnder modulator[C]. Optical Fiber Communication-Incudes Post Deadline Papers, 2009. 1-3.

4 Y Yang, C Lu, A P T Lau, *et al*.. A robust and dither-free technique for controlling driver signal amplitude for stable and arbitrary optical phase modulation [J]. Opt Express, 2011, 19(27): 26353-26358.

5 Y Yang, L Cheng, Z Li, *et al*.. An optical differential 8-PSK modulator using cascaded QPSK modulators[C]. Opt Commun, 2009. 1-2.

6 G W Lu, T Sakamoto, T Kawanishi. Rectangular QPSK for generation of optical eight-ary phase-shift keying [J]. Opt Express, 2011, 19(19): 18479-18485.

7 G W Lu, T Sakamoto, A Chiba, *et al*.. Reconfigurable multilevel transmitter using monolithically integrated quad Mach-Zehnder IQ modulator for optical 16-QAM and 8-PSK generation [J]. Opt Express, 2011, 19(6): 5596-5601.

8 S Tibuleac, M Filer. Transmission impairments in DWDM networks with reconfigurable optical add-drop multiplexers[J]. J Lightwave Technol, 2010, 28(4): 557-598.

9 Y Yang, L Cheng, Z Li, *et al*.. Strong optical filtering on direct detection NRZ differential 8-PSK (D8PSK) systems[C]. Opto-Electronics and Communications Conference, 2010. 288-289.

10 H M Nguyen, K Igarashi, K Katoh, *et al*.. Tunable optical equalizer for 40-Gbps intensity-modulated signal using PLC-based finite-impulse-response filter[C]. Opt Commun, 2010. 1-3.

11 J X Cai, O Sinkin, H Zhang, *et al*.. ISI compensation up to Nyquist channel spacing for strongly filtered PDM RZ QPSK using multi-tap CMA [C]. Optical Fiber Communication Conference, 2012.

12 Y Cai, J X Cai, A Pilipetskii, *et al*.. Spectral efficiency limits of pre-filtered modulation formats[J]. Opt Express, 2010, 18(19): 20273-20281.

13 C Kim, G Li. Direct-detection optical differential 8-level phase-shift keying (OD8PSK) for spectrally efficient transmission[J]. Opt Express, 2004, 12(15): 3415-3421.

14 B Mikkelsen, C Rasmussen, P Mamyshev, *et al*.. Partial DPSK with excellent filter tolerance and OSNR sensitivity[J]. Electron Lett, 2006, 42(23): 1363-1364.

栏目编辑：王晓琰